Microfluidics and Nanofluidics (2019) 23:16
https://doi.org/10.1007/s10404-018-2184-8

RESEARCH PAPER

Circular-channel particle focuser utilizing viscoelastic focusing

Nan Xiang[1] · Qing Dai[1] · Yu Han[1] · Zhonghua Ni[1]

Received: 6 October 2018 / Accepted: 27 December 2018 / Published online: 9 January 2019

Abstract
The miniaturization of flow focuser is a challenge in developing microflow cytometers. Most previously reported microfluidic cell focusers require complex structures or external force fields to achieve the 3D cell focusing. Herein, we propose a novel circular-channel particle focuser utilizing viscoelastic focusing. The circular-channel particle focuser is fabricated using a simple and low-cost microwire molding technique. Whole PDMS channels with perfect circular cross-sections can be fabricated using this protocol. We then characterize the particle focusing performances in our circular-channel particle focuser and discuss the effects of particle size, operating flow rate, cross-sectional dimension and fluid rheological property on particle focusing. The experimental results show that a perfect single-line focusing can be achieved exactly at the channel centerline. Finally, our circular-channel particle focuser is employed for the focusing of blood cells. As it offers special advantages of simple structure, easy fabrication, and sheathless operation, our circular-channel particle focuser may serve as a potential flow focuser for microflow cytometers.

Keywords Viscoelastic focusing · Circular channel · Single-line focusing · Microflow cytometer

1 Introduction

Flow cytometry has been widely employed for the diagnosis of various human diseases and expanded for many other applications in basic biological researches and clinical trials (Muirhead et al. 1985). One of its key components is the flow focuser which focuses the cells into a string so that the cells can pass through the downstream optical or electrical interrogation point one by one. In traditional flow cytometers, the sample fluid in the central core is pinched by the outer co-flow sheath fluid via a cuvette or nozzle fluidic system. Due to the pinching effect of sheath flow, the cells flowing in the sample flow can be gradually focused into a cell string, which is known as the hydrodynamic focusing (Steinkamp 1984). Recently, with the advent of microfabrication, the microflow cytometer has been successfully invented and attached increasing interests due to the offered special advantages of low sample consumption, small footprint and low hardware cost (Ateya et al. 2008; Piyasena and Graves 2014; Sun and Morgan 2010). Researchers have made sustained efforts to develop smaller optics, electric circuits and sensors for the next generation microflow cytometer.

One of the major challenges is the miniaturization of flow focuser as it is directly responsible for processing a huge number of cells with varied properties (size, shape, deformability, etc.) and requires to work in a high-throughput manner without clogging. The microfluidics (Whitesides 2006), which is capable of accurately manipulating the micro/nanoscale objects, offers a potential tool for addressing this challenge. The first generation microfluidic focuser inherited the design idea of hydrodynamic focusing using sheath flows (Lee et al. 2006; Simonnet and Groisman 2005). Due to the planar structure, the early microfluidic focuser can only achieve the two-dimensional (2D) focusing, that is the cells are focused into a band parallel to the channel side walls. This 2D hydrodynamic focusing may cause the detection errors due to the simultaneous existence of multiplex cells in the interrogation region. To realize the true

This article is part of the topical collection "Particle motion in non-Newtonian microfluidics" guest edited by Xiangchun Xuan and Gaetano D'Avino.

✉ Nan Xiang
nan.xiang@seu.edu.cn

Zhonghua Ni
nzh2003@seu.edu.cn

[1] School of Mechanical Engineering, and Jiangsu Key Laboratory for Design and Manufacture of Micro-Nano Biomedical Instruments, Southeast University, Nanjing 211189, China

three-dimensional (3D) focusing, additional sheath flow was introduced to pinch the sample flow in the vertical direction at the expense of device complexity and fabrication cost (Chang et al. 2007; Yang et al. 2005). Another active strategy for controllable cell focusing is based on the external fields (e.g., electric (Zhu et al. 2009), magnetic (Chen et al. 2018), optical (Zhao et al. 2007) and acoustic (Ding et al. 2013) fields). These active schemes own a high-focusing resolution, but require expensive external force-field generators. Recently, the passive inertial (Amini et al. 2014; Zhang et al. 2016) and viscoelastic focusing (D'Avino et al. 2017; Lu et al. 2017; Yuan et al. 2018) have attached increasing interests due to the offered advantages of easy operation and simple channel structure.

As compared with inertial focusing, the viscoelastic focusing only relies on the inherent viscoelasticity of fluid and offers a high focusing resolution up to nanoscale [e.g., the focusing of nanoparticles (Liu et al. 2016), DNA macromolecules (Kim et al. 2012) and exosomes (Liu et al. 2017)]. Up until now, experimental and numerical studies have demonstrated the viscoelastic focusing and the separation of particles/cells in channels with various geometries or cross-sectional shapes (e.g., rectangular and circular). (Lu et al. 2017; Tian et al. 2018; Yuan et al. 2018) Among the employed channels, the circular channel (i.e., channels with circular cross-sections) is certainly the most ideal one for viscoelastic focusing as the particles/cells flowing in circular channels occupy a stable equilibrium position at the channel center over a wide range of flow rates (D'Avino et al. 2012; Kang et al. 2013; Lu et al. 2017; Romeo et al. 2013; Yuan et al. 2018). However, the circular channel is difficult to be fabricated using the well-established soft lithography technique (Xia and Whitesides 1998). The few viscoelastic focusing experiments in circular channels (Asghari et al. 2017; D'Avino et al. 2012; Kang et al. 2013; Nam et al. 2015) were carried out using commercial glass capillaries which are very easy to break and difficult to be integrated with other lab-on-a-chip (LOC) components. In microelectromechanical system (MEMS) compatible rectangular channels, the particles/cells equilibrate at five cross-sectional positions at an extremely low flow rate (Seo et al. 2014; Yang et al. 2012), which prevents its application for downstream detection or separation. One simple method to address this issue is to appropriately increase the flow rate, which makes the coupling of the elastic effect with the inertial effect and reduces the original five equilibrium positions to the only one at the channel cross-sectional center (Del Giudice et al. 2017; Yang et al. 2011). However, this single-position focusing could only be achieved in a very narrow flow-rate regime and a standard square cross-section is required. For channels with a rectangular cross-section, multi-string focusing in the vertical center plane was generated due to the anisotropic flow field. (Liu et al. 2015; Xiang et al. 2016a).

In this work, we propose a whole polydimethylsiloxane (PDMS) circular-channel focuser for single-line viscoelastic focusing of particles/cells. The proposed circular-channel particle focuser is fabricated via the microwire molding technique without the assistance of complex alignment and bonding processes or complicated fabrication instruments. Then, the particle focusing performances in the fabricated circular-channel particle focuser are characterized via a series of experiments. Finally, the circular-channel particle focuser is employed for achieving the focusing of blood cells. We envision that our circular-channel particle focuser may serve as a potential unit for microflow cytometer.

2 Basic physics and working principle

Particles flowing in viscoelastic flows will migrate across the main streamlines due to the suffered nonlinear viscoelasticity of the suspending medium, which was discovered in macroscopic channels by Karnis and Mason (1966) and then first developed into the microscale flow in 2007 (Leshansky et al. 2007). The physics for this phenomenon is the first and second normal stress differences ($N_1(\dot{\gamma})$ and $N_2(\dot{\gamma})$) induced in viscoelastic fluids (D'Avino et al. 2012). The $\dot{\gamma}$ is the shear rate and can be estimated as $\dot{\gamma}(r) = -4Qr/\pi R^4$ for circular channels, where Q is the volume flow rate, r is the radial distance away from the channel centerline and R is the radius of the circular channel. For most viscoelastic fluids, the first normal stress difference will dominate over the second normal stress difference and can be approximated as $N_1(\dot{\gamma}) = \psi_1(\dot{\gamma})\dot{\gamma}^2$, where $\psi_1(\dot{\gamma})$ is the stress coefficient (Karimi et al. 2013). Within the shear rate range ($\dot{\gamma} < 1000\text{s}^{-1}$), the 8 wt% poly (vinyl pyrrolidone) (PVP) solutions employed in this work exhibit nearly constant viscosities (without significant shear thinning or thickening) (D'Avino et al. 2012) and can be regarded as Boger fluid (James 2009). For Boger fluids, the scaling of the first normal stress difference can be given as $N_1(\dot{\gamma}) \sim \eta\lambda\dot{\gamma}^2$ (where η is the zero-shear viscosity of fluids and λ is the relaxation time of fluids) (James 2009). For the 0.05 wt% poly (ethylene oxide) (PEO) viscoelastic solutions, a shear thinning phenomenon was observed at shear rates larger than 100 s^{-1} (D'Avino et al. 2012).

Due to the existence of $N_1(\dot{\gamma})$, the flowing particles will migrate towards the positions where the shear rates are at the minimum (Lu et al. 2017). As illustrated in Fig. 1a, in rectangular channels, there exist five positions where the shear rates are at the minimum (i.e., four corners and one center). Instead, in circular channels, the shear rate is in directly proportional to the radial distance (r) and is zero at the channel cross-sectional center (see Fig. 1a). Therefore, in

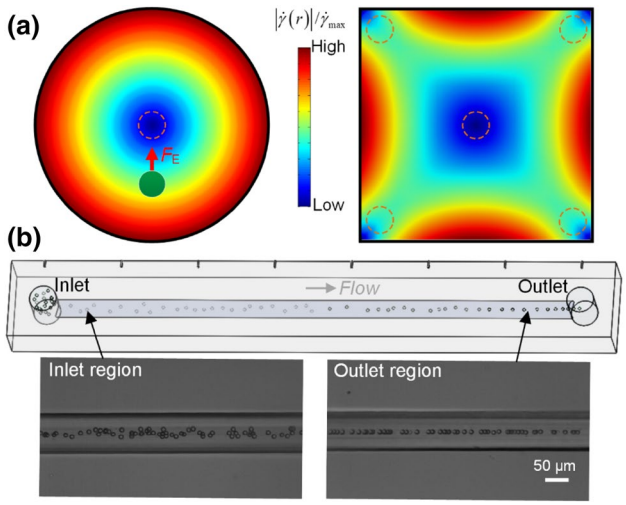

Fig. 1 **a** Shear-rate distributions and particle equilibrium positions in the cross-sections of a circular channel and a rectangular channel. **b** Particle focusing in viscoelastic flows in circular channels. Particles randomly dispensed near the inlet will gradually focus into a perfect single string exactly at the channel centerline when arriving at the outlet

viscoelastic flows, the particles will aggregate at the cross-sectional center in circular channels. As illustrated in Fig. 1b, the particles randomly dispensed near the inlet will gradually focus into a perfect single string when arriving at the outlet. The mechanics for this particle centerline focusing is the elastic force ($F_E \sim a_p^3 \frac{\partial N_1}{\partial r}$, where a_p is the particle diameter) which forces the particles towards the channel centerline (Xiang et al. 2016b). Through introducing the elastic coefficient (C_E) and the scaling of $N_1(\dot{\gamma})$ into the above equation, we can derive the force expression as $F_E = C_E a_p^3 \lambda \eta r Q^2 / R^8$. To characterize the fluid elastic effect, the Weissenberg number ($Wi = \lambda \dot{\gamma}_c$) can be employed (Li et al. 2016). The $\dot{\gamma}_c$ is the characteristic shear rate and can be calculated as $\dot{\gamma}_c = Q/2\pi R^3$ for circular channels.

At increased flow rates, the fluid inertial effect will also contribute to the particle focusing. A direct method to access the fluid inertial effect is the use of Reynolds number ($Re = 2\rho Q/\pi R\eta$, where ρ is the fluid density) (Squires and Quake 2005). The mechanics basis for this effect is the inertial lift force which has two components (Xiang et al. 2015; Zhang et al. 2014, 2016). When the particles approach the wall, a wall-induced inertial lift force (F_{WL}) due to the particle–wall interaction will push the particles away from the wall towards the channel center. At off-wall regions, the particles will suffer from the shear-induced inertial lift force (F_{SL}) whose direction is opposite to those of the F_{WL} and F_E. For particles at non-wall regions, the net inertial lift force (F_L) can be approximated as F_{SL} [$F_L \approx F_{SL} = C_L \rho Q^2 a_p^3 / 2\pi^2 R^5$, where the C_L is the lift coefficient and its magnitude is heavily dependent on the particle position (r) and Reynolds number (Re)] (Amini et al. 2014). The competition between the elastic effect and the inertial effect can be evaluated using the dimensionless Elasticity number ($El = Wi/Re = \lambda\eta/4\rho R^2$) (Lu et al. 2017; Yuan et al. 2018).

3 Result and discussion

3.1 Fabrication of the circular-channel particle focuser

The fabrication of circular channel remains a great challenge in MEMS process. Up until now, various methods [e.g., mechanical micromilling (Wilson et al. 2011), chemical etching (Grosse et al. 2001), photoresist melting (Wang et al. 2007), liquid metal amalgamating (Yan et al. 2018)] have been proposed to create master molds for casting microchannels with bell-shaped or semicircular cross-sections. Other methods to directly fabricate circular channels in bulk materials (e.g., glass and polymer) include 3D-printing (Wu et al. 2011) and femtosecond laser writing (He et al. 2010). However, these methods may require additional alignment and bonding steps or complicated fabrication instruments. In addition, perfect circular channels are difficult to achieve using these methods due to the bonding and fabrication errors. To rapidly and simply fabricate our circular-channel particle focuser, we employed the microwire molding process which is able to create channels with perfect circular cross-sections in bulk PDMS. As illustrated in Fig. 2a, the whole fabrication process can be completed within six simple steps. A detailed description of the fabrication process can be found as follow.

First, the selected microwires with determinate diameters were respectively cleaned with isopropanol and DI water in an ultrasonic washer for over 8 min. In this work, commercially available stainless steel microwires (with diameters of 50, 80, 100 and 150 μm) and nylon microwires (with diameters of 74, 105, 148 and 181 μm) purchased from local market were selected and employed. After being dried with nitrogen gas, these microwires were tightened up and fixed in a custom mold (see Fig. 2b). The use of our custom mold enables the easy alignment of multiplex microwires at a time. Then, the microwires were served as the master molds to carry out the well-established PDMS micromolding process. Specifically, the totally mixed PDMS mixture (Sylgard 184, Dow Corning) with the weight ratio of base to curing agent of 10:1 was casted into the custom mold. After curing at 80 °C for 2 h, the PDMS block was cut off from the custom mold and immersed into the alcohol for 6 h (the use of ultrasonic oscillation can help reduce this time). Due to the swelling effect of PDMS in organic solvent, the microwires can be easily pulled out from the PDMS block.

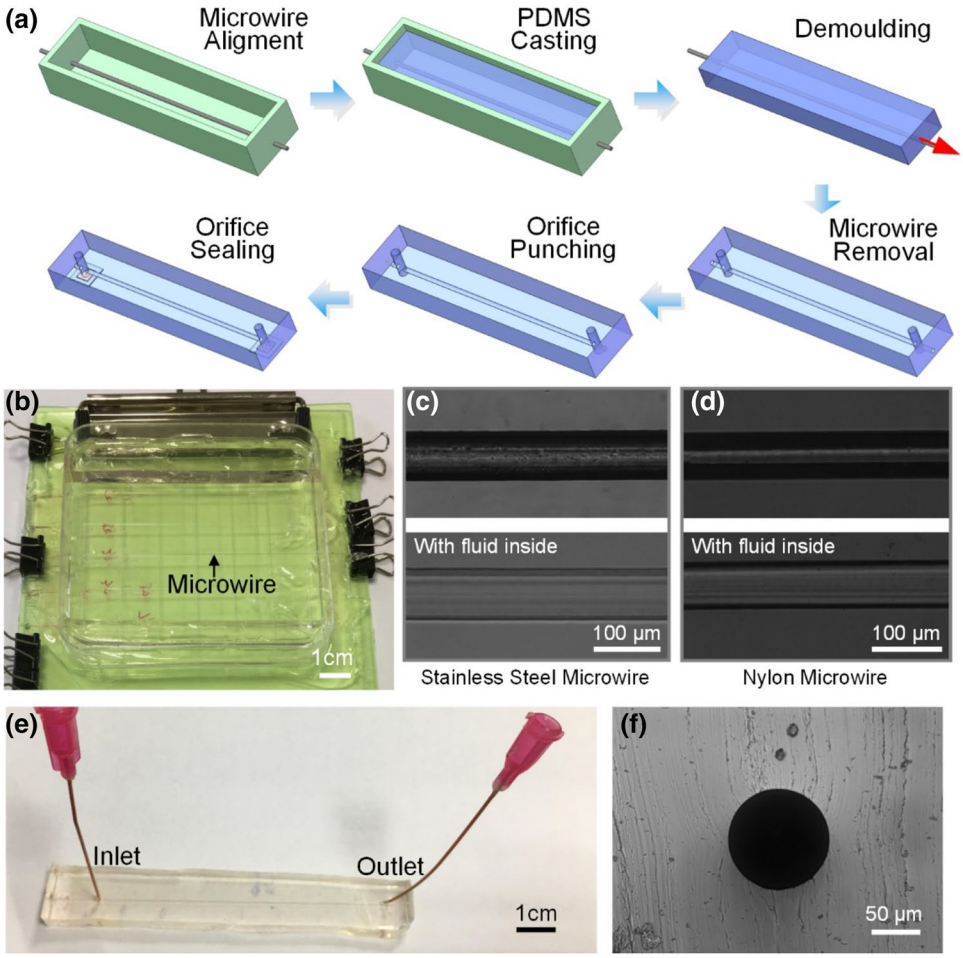

Fig. 2 **a** Schematic diagram of the process for fabricating our circular-channel particle focuser. **b** The custom mold for aligning the microwires. **c, d** Microscopic images illustrating the circular channel fabricated using the stainless steel microwire (**c**) and the nylon microwire (**d**). The lower images illustrate the fabricated channels with fluid inside. **e** Photograph of the fabricated circular-channel particle focuser. The inlet and outlet orifices were inserted with tubing for sample introduction and exportation. **f** Cross-sectional profile of the fabricated circular-channel particle focuser

It is noticed that too long immersion time will lead to a large dimension deviation. After creating a circular channel in the bulk PDMS, the inlet and outlet orifices were punched using the needle of a luer stub adapter. Finally, a small amount of liquid PDMS was used to seal the orifices at the bottom surface and the channel ends via the capillarity. Figure 2c, d shows the microscopic images illustrating the circular channels fabricated using stainless steel microwires and nylon microwires. After pumping the liquid through, the fabricated microchannel shows a good optical property, which makes the downstream optical detections [e.g., laser-induced fluorescence detection (Chabinyc et al. 2001) and high-throughput image-based screening (Otto et al. 2015)] to be possible. Figure 2e shows the photograph of a fabricated circular-channel particle focuser with a cross-section diameter of 79 μm. As there is no rigid material (e.g., glass slide) been used, our circular-channel focuser can be easily mounted onto any surface or be integrated with other LOC components. Figure 2f illustrates the cross-sectional profile of the fabricated circular-channel particle focuser. As can be seen from this figure, a perfect circular cross section can be obtained using the above microwire molding method.

3.2 Characterization of particle focusing performances

After successfully fabricating our circular-channel particle focuser, we next characterized its particle focusing performances to guide the potential applications. To probe into the effect of flow rate on particle focusing, we respectively pumped the 10 μm and 5 μm particle suspensions added with 8 wt% PVP into the fabricated particle focuser with a diameter of 79 μm at the flow rates of 1–60 μl/min. Figure 3a illustrates the focusing maps of these two particles near the outlet (at a distance of ~ 5 cm away from the inlet) at different flow rates. As can be seen from these two focusing maps, the 10 μm large particles show a much better focusing performance than the 5 μm small particles. The 10 μm particles can focus into a single-stream at the beginning flow rate of 1 μl/min and keep single-stream focusing over the whole tested flow rate range while the 5 μm particles can only migrate to form a relatively wide particle band at all tested flow rates. This observation can be explained as the difference in elastic forces which are directly proportional to the particle diameter ($F_E \sim a_p^3$).

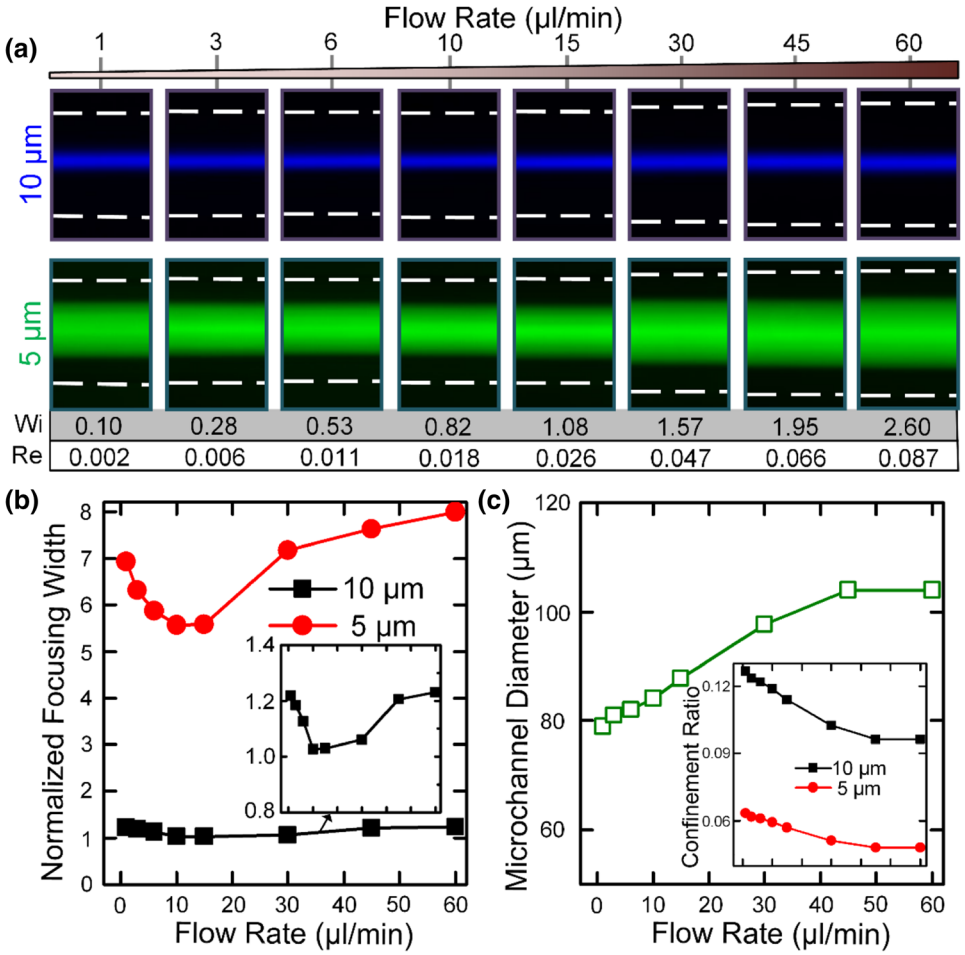

Fig. 3 **a** Focusing maps of 10 μm and 5 μm particles at different flow rates of 1–60 μl/min. The white dotted lines illustrate the walls of the channel. **b** Normalized focusing widths of these two-sized particles as a function of flow rate. The inset is the enlarged figure with a small vertical scale (0.8–1.4). **c** The measured microchannel diameter at different flow rates. The PDMS channel will expand from 79 to 104 μm due to the increased flow pressure. The inset shows the variation of confinement ratios with increasing flow rate. The abscissa is the same with the large figure

The elastic forces acting on 5 μm small particles are insufficient for forcing all the particles (especially the particles with their initial positions close to the channel wall) towards the channel centerline within a finite channel length. The focusing of small particles or even sub-micro/nano particles can be realized through decreasing the channel cross-sectional dimension or increasing the channel length. The calculated *Wi* and *Re* for the current flow regime are respectively 0.10–2.60 and 0.002–0.087. The small Re ($Re << 1$) indicates that the fluid inertial effect can be neglected in the current experiment and the particle migration will be completely dominated by the elastic effect. For rectangular channels, the single-stream focusing can only be achieved within a very narrow flow rate regime where the elastic effect will be coupled with the inertial effect (i.e., elasto-inertial focusing under $Re > 1$ and $Wi > 1$) (Xiang et al. 2016a; Yang et al. 2011). Instead, in our circular-channel particle focuser, particles of specific sizes (e.g., 10 μm particles in this work) can be single-line focused exactly at the channel centerline under an extremely small Re, and keep this focusing status over a wide flow rate range.

To quantify the particle focusing performances, we defined the normalized focusing width through dividing the measured full width at half maximum (FWHM) of the fluorescent intensity profile by particle diameter. Figure 3b shows the normalized focusing widths of 10 μm and 5 μm particles at different flow rates. As can be seen from these two curves, the 10 μm particle streams have small normalized focusing widths of around 1 at all tested flow rates while the normalized focusing widths are all larger than 5.5 for 5 μm particles due to the insufficient focusing. In addition, we found that the normalized focusing width will firstly decrease and then gradually increase with increasing flow rate. The optimal flow rates of the two-sized particles for achieving the best focusing performances are both 10 μl/min. Under the optimal flow rate, the normalized focusing widths for 10 μm and 5 μm particles are, respectively, 1.03 and 5.56. The physics for the focusing enhancement at low flow rates is the strengthen of elastic forces with increasing flow rate ($F_E \sim Q^2$). At high flow rates, the channel expansion under the high pressures (see Fig. 3c) will also weaken the focusing performance. To analyze this phenomenon, the confinement ratio ($\beta = a_p/2R$) was defined and employed

(the confinement ratios at different flow rates are illustrated in the inset of Fig. 3c). With the increasing of flow rate, the confinement ratio will gradually decrease for both two-sized particles. Therefore, the deterioration of the focusing performance at high flow rates can be explained as the decrease of confinement ratios due to the channel expansion (Romeo et al. 2013). The channel expansion is the major limitation of our circular-channel particle focuser. The same problem has also been observed in previously reported PDMS devices when dealing with high viscous (Del Giudice et al. 2016) or high-speed inertial flows (Sollier et al. 2011). One potential method to address this issue is the using of more rigid PDMS (with a higher ratio of curing agent to base) or other rigid polymers. A more detailed discussion on the effect of channel deformation on particle migration in the flow of viscous polymer solutions can be found in a previous microrheometry study (Del Giudice et al. 2016).

In addition to the above-employed 79 μm diameter channel, we fabricated two additional channels with initial diameters of 100 μm and 152 μm. The 8 wt% PVP solutions mixed with 10 μm particles were, respectively, pumped into these two channels. The confinement ratios (β) for these two channels are respectively 0.100 (for 100 μm channel) and 0.066 (for 152 μm channel). Figure 4a illustrates the focusing maps near the outlet under both fluorescent and bright-field modes. Figure 4b shows the normalized focusing widths in these two channels as a function of flow rate. From the above experimental results, we found that the focusing performance will worse with increasing channel diameter as the elastic force is inversely proportional to the channel diameter ($F_E \sim R^{-8}$). For the 100 μm diameter channel ($\beta = 0.100$), the variation trend of particle focusing is very similar to that observed in the 79 μm diameter channel ($\beta = 0.127$) and the optimal normalized focusing width of 1.66 can be achieved at a flow rate of 25 μl/min. In the 152 μm large diameter channel ($\beta = 0.066$), although the focusing performance will be gradually enhanced, the particles could not focus into a narrow stream at all flow rates, which is similar to the observed phenomenon of 5 μm small particles in the 79 μm diameter channel ($\beta = 0.063$) as they have similar confinement ratios. Under the highest tested flow rate ($Q = 50$ μl/min, $Wi = 0.7$ and $Re = 0.05$), the normalized focusing width is 5.31, which is insufficient for ensuring the accuracy of downstream detection.

To explore the effect of fluid rheological property on particle focusing performance, an additional experiment using 0.05 wt% PEO solutions mixed with 10 μm particles was carried out. The channel diameter for this experiment was selected to be 79 μm. Figure 5a illustrates a comparison of particle focusing images in these two viscoelastic solutions. Figure 5b shows the normalized focusing widths of particle focusing in these two viscoelastic solutions as a function of flow rate. From these experimental results, we found that the particles flowing in the 0.05 wt% PEO solution show a slightly better focusing performance than that in the 8 wt% PVP solution at flow rates below 30 μl/min due to the long relaxation time of 0.05 wt% PEO solution. The optimal normalized focusing width can be as low as 0.76, which means the FWHM of the particle focusing stream is even smaller than the particle diameter. As the observed uniform particle shadings, we concluded that a true channel-centerline focusing can be achieved in our circular-channel particle focuser. Further increasing the flow rate to be higher than 30 μl/min, the normalized focusing widths of particles in 0.05 wt% PEO solution sharply increase and surpass the values in 8 wt% PVP solutions due to the occurrence of multi-position focusing. Different from the defocusing caused by the channel deformation in the above experiment using high viscosity 8 wt% PVP solutions, the channel deformation in this experiment is very small even at the highest tested flow rate. The possible reason for the multi-position defocusing is the increased contribution of inertial effect on particle focusing.

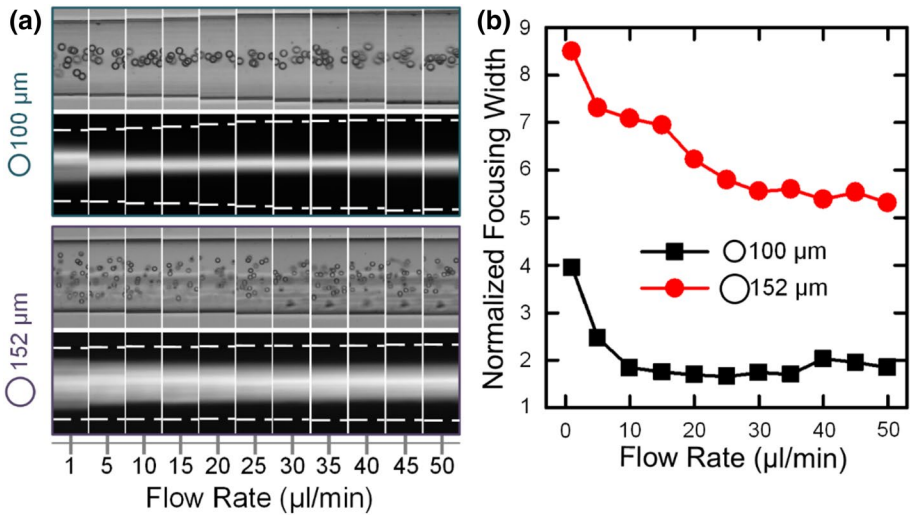

Fig. 4 **a** Focusing maps of 10 μm particles flowing in 100 μm ($\beta = 0.100$) and 152 μm ($\beta = 0.066$) diameter channels at different flow rates of 1–50 μl/min. For each channel, the top row is the overlaid bright-filed images and the bottom row is the overlaid fluorescent images. The white dotted lines in the fluorescent images mark the positions of channel walls. **b** The normalized focusing widths in these two channels as a function of flow rate

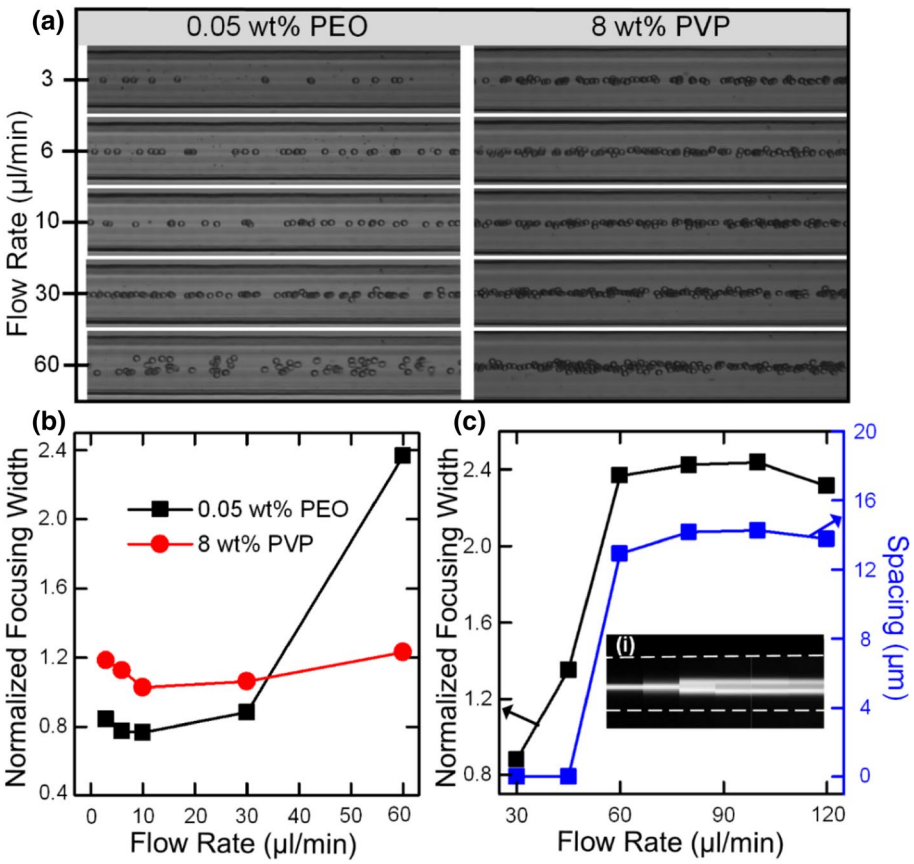

Fig. 5 **a** Focusing maps of 10 μm particles in the 0.05 wt% PEO solution and the 8 wt% PVP solution at different flow rates of 3–60 μl/min. **b** The normalized focusing widths of particles flowing in these two viscoelastic solutions as a function of flow rate. **c** The normalized focusing widths and the spacings between the two focused streams in the 0.05 wt% PEO solution at high flow rates of 30–120 μl/min. The inset (i) in this figure illustrates the focusing map at high flow rates. The white dotted lines mark the channel walls

To access the competition between the elastic effect and the inertial effect, the dimensionless Elasticity number (El) was calculated. For the 8 wt% PVP solution, the El was calculated to be 51.73 (this value was calculated using the channel diameter before deformation) while a much smaller El of 4.56 was achieved for the 0.05 wt% PEO solution. The small El of order 1 (El ~ O (1)) indicates that the particles in the 0.05 wt% PEO solution will be easily inferenced by the non-ignorable inertial effect at high flow rates ($Re > 1$ at the flow rate larger than 30 μl/min). Under the coupling of the elastic effect and the inertial effect, the particles will focus at multi-positions, which was also observed in the previously reported particle focusing in rectangular channels (Liu et al. 2015; Xiang et al. 2016a). In addition, the shear-thinning effect of the 0.05 wt% PEO solution at shear rates larger than 100 s^{-1} will force the particle towards the channel wall (the shear rate is 1295 s^{-1} at the flow rate of 30 μl/min).

To characterize the multi-position defocusing, we further increased the flow rate to 120 μl/min. Figure 5c illustrates the normalized focusing widths and the spacings between the two focused streams at high flow rates of 30–120 μl/min. For calculating the focusing width, the two streams were treated as a single large stream. The distance between the two peaks of intensity profiles was defined as the spacing between the two streams. The insert (i) of Fig. 5c is the focusing maps illustrating the generation process of the multi-stream at high flow rates. It is found that the normalized focusing width and spacing will first increase and then be constant at a specific value when the flow rate is large than 60 μl/min.

3.3 Application for biological cell focusing

After characterizing the performances of our circular-channel particle focuser, we next explored its practicability for processing biological cells. Human whole blood, the most frequently employed sample in the flow cytometry, was tested in this experiment. To focus the broad-sized blood cells (red blood cells of ~ 6 μm and white blood cells of 10–15 μm), a circular-channel particle focuser with a diameter of 79 μm and a channel length of 5 cm was fabricated and employed. The 0.05 wt% PEO-PBS solution was employed as the viscoelastic fluid for the focusing of blood cells. To ensure an acceptable focusing performance, the blood sample was diluted with the prepared PEO–PBS solution for 100 times so that the cell–cell interactions can be significantly reduced. Then, the prepared blood cell suspensions were respectively injected into our circular-channel particle focuser at different flow rates of 6–100 μl/min. The cell distributions across the channel width near the outlet were

captured under the bright-field mode and over 50 individual focusing images were vertically overlaid. Figure 6a groups the composite focusing images illustrating the focusing performances of blood cells at different flow rates. As can be seen from this focusing map, the blood cell can successfully focus into a cell string exactly at the channel centerline at the flow rates of 6 µl/min and 10 µl/min. After that, the width of cell focusing band will gradually increase with increasing flow rate. To quantitatively illustrate the focusing performance, we measured the widths of cell bands across the channel width at different flow rates, and the result is illustrated in Fig. 6b. The cell band width achieves the minimum of ~ 7 µm at the flow rate of 10 µl/min. These results well indicate that our circular-channel particle focuser can be successfully employed for the focusing of blood cells.

The throughput of our circular-channel particle focuser is lower than previously reported inertial microfluidics (Amini et al. 2014), but a perfect single-line focusing can be easily realized using our simple focuser. For most inertial microfluidics, there exists multiplex equilibrium positions, which may cause the detection error due to the simultaneous existence of multiplex cells in the detection region. For example, the curved inertial microfluidics actually has two vertical equilibrium positions which overlap with each other from the top view (Jiang et al. 2016). In addition to the centerline focusing, our circular-channel particle focuser offers additional advantages such as simple structure, easy fabrication, sheathless and label-free operation. The throughput of our circular-channel particle focuser can be further increased for practical applications through paralleling of multiplex focusers or using the HA or DNA as the elasticity enhancer. In addition, the pre-sorting of undiluted blood samples using viscoelastic focusing may be another approach for increasing the throughput of downstream focusing/counting (Tian et al. 2018).

4 Conclusion

In this work, a circular-channel particle focuser is proposed to realize the single-line focusing of particles/cells utilizing the viscoelastic focusing. The proposed circular-channel particle focuser is fabricated via microwire molding technique. Using this method, various channels with perfect circular cross-sections can be fabricated without complex alignment and bonding processes or complicated fabrication instruments. The fabricated channels have a good optical property and offer various cross-sectional dimensions. To better understand our circular-channel particle focuser, the particle focusing performances are characterized via a serial of experiments. The experimental results prove that our circular-channel particle focuser is capable of focusing particles exactly at the channel centerline over a relatively broad flow rate range. In addition, the effects of flow rate, particle size, channel dimension and fluid rheological property on particle focusing are explored. These findings will provide valuable insights for a better understanding and operating of our circular-channel particle focuser. To examine the practicability of our circular-channel particle focuser, we employ the focuser for the focusing of blood cells. We envision that our circular-channel particle focuser may serve as a potential unit for microflow cytometer.

5 Methods

5.1 Preparation of viscoelastic fluids

Two viscoelastic fluids (8 wt% PVP and 0.05 wt% PEO solutions) employed in this work were prepared by dissolving the polymer powder of poly (vinyl pyrrolidone) (PVP, molecular weight M_w = 360 KDa, Sigma-Aldrich) and

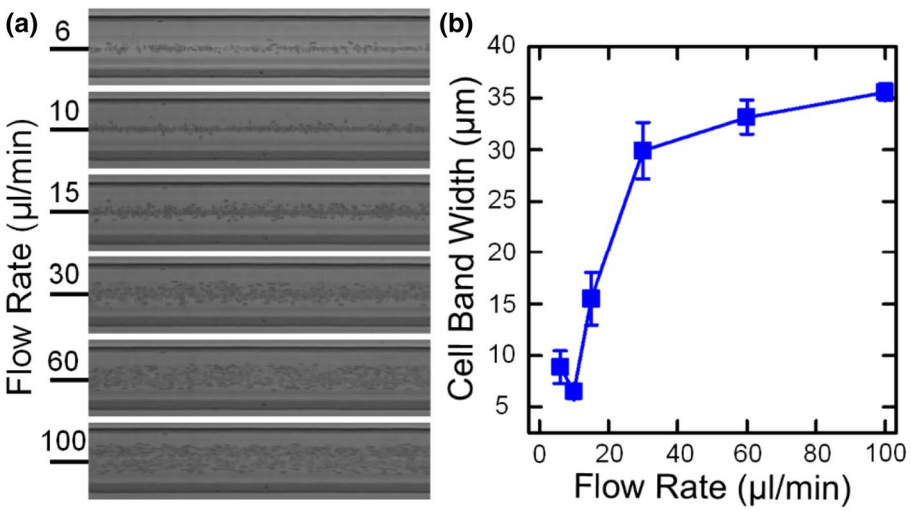

Fig. 6 **a** The focusing images of blood cells at different flow rates of 6–100 µl/min. **b** The measured cell band widths at different flow rates

poly (ethylene oxide) (PEO, molecular weight $M_w = 2000$ KDa, Sigma-Aldrich) in deionized (DI) water, respectively. For the 0.05 wt% PEO solution, 22 wt% glycerin (Sigma-Aldrich) was mixed into the aqueous solution for the purpose of adjusting fluid density. The relaxation time (λ) and zero-shear viscosity (η) of the prepared 8 wt% PVP solution are, respectively, 2.3 ms and 140 mPa s according to the experimental values in the previous study (Yang et al. 2011). Meanwhile, for the 0.05 wt% PEO solution, a longer relaxation time (λ) of 9.1 ms and a lower viscosity (η) of 3.12 mPa s can be achieved due to the high molecular weight of the PEO additive.

The relaxation time of this low concentration PEO solution was estimated using the empirical formula as it was difficult to be accurately measured through experimental approaches. The detailed calculation method can be found in our previous study (Xiang et al. 2016b). All these two polymer additives have been previously proved to be compatible with biological cells (Yuan et al. 2018).

Then, we respectively mixed two fluorescent polymer particles (Product Nos. G1000 and G0500, Thermal Scientific) with different sizes of 10 μm and 5 μm into the prepared two viscoelastic fluids. For blood cell experiments, the human whole blood was diluted using the phosphate-buffered saline (PBS, Sigma-Aldrich) dissolving with 0.05 wt% PEO powder. Human whole blood was draw from a healthy consenting volunteer using a vacutainer collection tube (BD Biosciences) containing anticoagulant K_2EDTA and used within 24 h. The concentrations of all the particle/cell suspensions were controlled to be very low so that the particle–particle interactions can be safely neglected. However, the detailed concentration values may vary in different experiments.

5.2 Experimental setup and data processing

The fabricated circular-channel particle focuser was mounted onto an inverted fluorescence microscope (IX 71, Olympus) for observing the particle focusing in channels. The particle motions were recorded using a CCD camera (Exi Blue, QImaging) under fluorescence or bright-filed modes and saved as image frames for further processing. The syringe pump (Legato 270, KD Scientific) was used to drive the sample liquid in an equipped 10 ml syringe at a specific and stable flow rate. The inlet orifice was connected with the syringe via a piece of PEEK tubing (Upchurch Scientific) and corresponding fittings. The outlet orifice was directly connected with a centrifuge tube for collecting the waste sample liquid. The experimental frames were processed using the free ImageJ software (NIH). To avoid the random errors, over 100 image frames were vertically stacked to generate the composite image illustrating the statistical particle distributions over a certain time period. The intensity profiles across the channel width were also measured using this software. The full width at half maximum (FWHM) of the intensity profiles were obtained through gaussian fitting. The FWHM normalized with particle diameter was defined as the particle focusing width. For blood cell experiments, the widths of the blood cell bands across the channel width were directly measured from the bright-field images.

Acknowledgements This research work is supported by the National Natural Science Foundation of China (81727801, 51875103, 51505082, and 51775111), the Natural Science Foundation of Jiangsu Province (BK20150606), the Fundamental Research Funds for the Central Universities (2242017K41031), the Six Talent Peaks Project of Jiangsu Province (SWYY-005) and the ZhiShan Young Scholar Fellowship.

References

Amini H, Lee W, Di Carlo D (2014) Inertial microfluidic physics. Lab Chip 14:2739–2761

Asghari M, Serhatlioglu M, Ortaç B, Solmaz ME, Elbuken C (2017) Sheathless microflow cytometry using viscoelastic fluids. Sci Rep 7:12342

Ateya DA, Erickson JS, Howell PB, Hilliard LR, Golden JP, Ligler FS (2008) The good, the bad, and the tiny: a review of microflow cytometry. Anal Bioanal Chem 391:1485–1498

Chabinyc ML, Chiu DT, McDonald JC, Stroock AD, Christian JF, Karger AM, Whitesides GM (2001) An integrated fluorescence detection system in poly (dimethylsiloxane) for microfluidic. Appl Anal Chem 73:4491–4498

Chang C-C, Huang Z-X, Yang R-J (2007) Three-dimensional hydrodynamic focusing in two-layer polydimethylsiloxane (PDMS) microchannels. J Micromech Microeng 17:1479

Chen Q et al (2018) Tunable, sheathless focusing of diamagnetic particles in ferrofluid microflows with a single set of overhead permanent magnets. Anal Chem 90:8600–8606

D'Avino G, Romeo G, Villone MM, Greco F, Netti PA, Maffettone PL (2012) Single line particle focusing induced by viscoelasticity of the suspending liquid: theory, experiments and simulations to design a micropipe flow-focuser. Lab Chip 12:1638–1645

D'Avino G, Greco F, Maffettone PL (2017) Particle migration due to viscoelasticity of the suspending liquid and its relevance in microfluidic devices. Annu Rev Fluid Mech 49:341–360

Del Giudice F, Greco F, Netti PA, Maffettone PL (2016) Is microrheometry affected by channel deformation? Biomicrofluidics 10:043501

Del Giudice F, Sathish S, D'Avino G, Shen AQ (2017) "From the edge to the center": viscoelastic migration of particles and cells in a strongly shear-thinning liquid flowing in a microchannel. Anal Chem 89:13146–13159

Ding X et al (2013) Surface acoustic wave microfluidics. Lab Chip 13:3626–3649

Grosse A, Grewe M, Fouckhardt H (2001) Deep wet etching of fused silica glass for hollow capillary optical leaky waveguides in microfluidic devices. J Micromech Microeng 11:257

He F et al (2010) Fabrication of microfluidic channels with a circular cross section using spatiotemporally focused femtosecond laser pulses. Opt Lett 35:1106–1108

James DF (2009) Boger fluids. Ann Rev Fluid Mech 41:129–142

Jiang D, Tang W, Xiang N, Ni Z (2016) Numerical simulation of particle focusing in a symmetrical serpentine microchannel. RSC Adv 6:57647–57657
Kang K, Lee SS, Hyun K, Lee SJ, Kim JM (2013) DNA-based highly tunable particle focuser. Nat Commun 4:2567
Karimi A, Yazdi S, Ardekani AM (2013) Hydrodynamic mechanisms of cell particle trapping in microfluidics. Biomicrofluidics 7:021501
Karnis A, Mason SG (1966) Particle motions in sheared suspensions. XIX. Viscoelast Media Trans Soc Rheol 10:571–592
Kim JY, Ahn SW, Lee SS, Kim JM (2012) Lateral migration and focusing of colloidal particles and DNA molecules under viscoelastic flow. Lab Chip 12:2807–2814
Lee G-B, Chang C-C, Huang S-B, Yang R-J (2006) The hydrodynamic focusing effect inside rectangular microchannels. J Micromech Microeng 16:1024
Leshansky A, Bransky A, Korin N, Dinnar U (2007) Tunable nonlinear viscoelastic "focusing" in a microfluidic device. Phys Rev Lett 98:234501
Li D, Lu X, Xuan X (2016) Viscoelastic separation of particles by size in straight rectangular microchannels: a parametric study for a refined understanding. Anal Chem 88:12303–12309
Liu C, Xue C, Chen X, Shan L, Tian Y, Hu G (2015) Size-based separation of particles and cells utilizing viscoelastic effects in straight microchannels. Anal Chem 87:6041–6048
Liu C, Ding B, Xue C, Tian Y, Hu G, Sun J (2016) Sheathless focusing and separation of diverse nanoparticles in viscoelastic solutions with minimized shear. thinning. Anal Chem 88:12547–12553
Liu C et al (2017) Field-free isolation of exosomes from extracellular vesicles by microfluidic viscoelastic flows. ACS Nano 11:6968–6976
Lu X, Liu C, Hu G, Xuan X (2017) Particle manipulations in non-Newtonian microfluidics: a review. J Colloid Interface Sci 500:182–201
Muirhead KA, Horan PK, Poste G (1985) Flow cytometry: present and future. Bio/Technology 3:337
Nam J, Tan JKS, Khoo BL, Namgung B, Leo HL, Lim CT, Kim S (2015) Hybrid capillary-inserted microfluidic device for sheathless particle focusing and separation viscoelastic flow. Biomicrofluidics 9:064117
Otto O et al (2015) Real-time deformability cytometry: on-the-fly cell mechanical phenotyping. Nat Methods 12:199
Piyasena ME, Graves SW (2014) The intersection of flow cytometry with microfluidics and microfabrication. Lab Chip 14:1044–1059
Romeo G, D'Avino G, Greco F, Netti PA, Maffettone PL (2013) Viscoelastic flow-focusing in microchannels: scaling properties of the particle radial distributions. Lab Chip 13:2802–2807
Seo KW, Kang YJ, Lee SJ (2014) Lateral migration and focusing of microspheres in a microchannel flow of viscoelastic fluids. Phys Fluids 26:063301
Simonnet C, Groisman A (2005) Two-dimensional hydrodynamic focusing in a simple microfluidic device. Appl Phys Lett 87:114104
Sollier E, Murray C, Maoddi P, Di Carlo D (2011) Rapid prototyping polymers for microfluidic devices and high pressure injections. Lab Chip 11:3752–3765
Squires TM, Quake SR (2005) Microfluidics: fluid physics at the nanoliter scale. Rev Mod Phys 77:977
Steinkamp JA (1984) Flow cytometry. Rev Sci Instr 55:1375–1400
Sun T, Morgan H (2010) Single-cell microfluidic impedance cytometry: a review. Microfluid Nanofluid 8:423–443
Tian F, Cai L, Chang J, Li S, Liu C, Li T, Sun J (2018) Label-free isolation of rare tumor cells from untreated whole blood by interfacial viscoelastic microfluidics. Lab Chip 18:3436–3445
Wang G-J, Ho K-H, Hsu S-h, Wang K-P (2007) Microvessel scaffold with circular microchannels by photoresist melting. Biomed Microdev 9:657–663
Whitesides GM (2006) The origins and the future of microfluidics. Nature 442:368
Wilson ME, Kota N, Kim Y, Wang Y, Stolz DB, LeDuc PR, Ozdoganlar OB (2011) Fabrication of circular microfluidic channels by combining mechanical micromilling and soft lithography. Lab Chip 11:1550–1555
Wu W, DeConinck A, Lewis JA (2011) Omnidirectional printing of 3D microvascular networks. Adv Mater 23:H178-H183
Xia Y, Whitesides GM (1998) Soft lithography. Annu Rev Mater Sci 28:153–184
Xiang N, Shi Z, Tang W, Huang D, Zhang X, Ni Z (2015) Improved understanding of particle migration modes in spiral inertial microfluidic devices. RSC Adv 5:77264–77273
Xiang N, Dai Q, Ni Z (2016a) Multi-train elasto-inertial particle focusing in straight microfluidic channels. Appl Phys Lett 109:134101
Xiang N, Zhang X, Dai Q, Cheng J, Chen K, Ni Z (2016b) Fundamentals of elasto-inertial particle focusing in curved microfluidic channels. Lab Chip 16:2626–2635
Yan S et al (2018) Liquid metal-based amalgamation-assisted lithography for fabrication of complex channels with diverse structures and configurations. Lab Chip 18:785–792
Yang R, Feeback DL, Wang W (2005) Microfabrication and test of a three-dimensional polymer hydro-focusing unit for flow cytometry applications. Sens Actuators A Phys 118:259–267
Yang S, Kim JY, Lee SJ, Lee SS, Kim JM (2011) Sheathless elasto-inertial particle focusing and continuous separation in a straight rectangular microchannel. Lab Chip 11:266–273
Yang S et al (2012) Deformability-selective particle entrainment and separation in a rectangular microchannel using medium viscoelasticity. Soft Matter 8:5011–5019
Yuan D, Zhao Q, Yan S, Tang S-Y, Alici G, Zhang J, Li W (2018) Recent progress of particle migration in viscoelastic fluids. Lab Chip 18:551–567
Zhang J, Yan S, Sluyter R, Li W, Alici G, Nguyen N-T (2014) Inertial particle separation by differential equilibrium positions in a symmetrical serpentine micro-channel. Sci Rep 4:4527
Zhang J, Yan S, Yuan D, Alici G, Nguyen N-T, Warkiani ME, Li W (2016) Fundamentals and applications of inertial microfluidics: a review. Lab Chip 16:10–34
Zhao Y, Fujimoto BS, Jeffries GDM, Schiro PG, Chiu DT (2007) Optical gradient flow focusing. Opt Express 15:6167–6176
Zhu J, Tzeng T-RJ, Hu G, Xuan X (2009) DC dielectrophoretic focusing of particles in a serpentine microchannel. Microfluid Nanofluid 7:751